

DETECTION OF OXYGEN AND CARBON IN THE HYDRODYNAMICALLY ESCAPING ATMOSPHERE OF THE EXTRASOLAR PLANET HD 209458B

A. VIDAL-MADJAR¹, J.-M. DÉSERT¹, A. LECAVELIER DES ETANGS¹, G. HÉBRARD¹,
 G. E. BALLESTER², D. EHRENREICH¹, R. FERLET¹, J. C. McCONNELL³, M. MAYOR⁴,
 C. D. PARKINSON⁵

Draft version August 9, 2018

ABSTRACT

Four transits of the planet orbiting the star HD 209458 were observed with the STIS spectrograph on board HST. The wavelength domain (1180–1710Å) includes H I as well as C I, C II, C IV, N V, O I, Si I, Si II, Si III and Si IV lines. During the transits, absorptions are detected in H I, O I and C II ($5\pm2\%$, $13\pm4.5\%$ and $7.5\pm3.5\%$, respectively). No absorptions are detected for other lines. The 5% mean absorption over the whole H I Lyman α line is consistent with the previous detection at higher resolution (Vidal-Madjar et al. 2003). The absorption depths in O I and C II show that oxygen and carbon are present in the extended upper atmosphere of HD 209458b. These species must be carried out up to the Roche lobe and beyond, most likely in a state of hydrodynamic escape.

Subject headings: Star: individual (HD 209458) – Stars: planetary systems

1. INTRODUCTION

The extrasolar planet HD 209458b is the first one for which repeated transits across the stellar disk have been observed ($\sim 1.5\%$ absorption; Henry et al. 2000; Charbonneau et al. 2000). Together with radial velocity measurements (Mazeh et al. 2000), this has led to a determination of the planet’s radius and mass, confirming that it is a gas giant. During transits, the Hubble Space Telescope (HST) allowed the detection of the dense lower atmosphere in the neutral sodium lines ($\sim 0.02\%$ additional absorption, Charbonneau et al. 2002) and the extended upper atmosphere in H I ($\sim 15\%$ absorption over the stellar Lyman α emission line, Vidal-Madjar et al. 2003). This H I absorption extends beyond the Roche lobe, showing a population of escaping atoms. The escape rate is estimated to be $\gtrsim 10^{10} \text{ g s}^{-1}$, consistent with theoretical evaluations (Hébrard et al. 2003, Lammer et al. 2003, Lecavelier des Etangs et al. 2004). The additional HST observations which we present here allow the upper atmosphere of HD 209458b to be further studied.

2. OBSERVATIONS AND DATA REDUCTION

Four transits of HD 209458b were surveyed with the STIS G140L spectrograph with four HST visits on Oct. 9, Oct. 21, Nov. 5 and Nov. 24, 2003. For each transit, three exposures during three consecutive HST orbits were scheduled such that at least one full exposure was obtained with the planet in front of the star. A previous or a following exposure, either entirely before the first contact or after the last contact, serves as a reference.

The resulting 1D and 2D spectra, output from the STIS pipeline, are similar to those described by Vidal-Madjar et al. (2003). In particular they show detectable geocoronal

emissions in H I and O I lines and a non-zero background level due to the dark current. To correct for these effects, we extracted the spectra from the 2D images of the detector following the procedure developed by Vidal-Madjar et al. (2003) and Désert et al. (2003). In each column of the detector we evaluate the background signal, including the geocorona, above and below the stellar spectrum and interpolate its value to be subtracted from the stellar spectrum. The errors due to the background and the geocorona are included in the error estimates.

The wavelength domain of the G140L first order grating ranges from 1180 Å to 1710 Å. The spectra are dominated by various stellar emission lines (Si III $\lambda 1206\text{\AA}$, H I $\lambda 1216\text{\AA}$, N V $\lambda 1239\text{\AA}$ and $\lambda 1243\text{\AA}$, O I $\lambda 1302\text{\AA}$, C II $\lambda 1335\text{\AA}$, Si IV $\lambda 1394\text{\AA}$ and $\lambda 1403\text{\AA}$, Si I $\lambda 1474\text{\AA}$, Si II $\lambda 1527\text{\AA}$, C IV $\lambda 1548\text{\AA}$ and $\lambda 1551\text{\AA}$, C I $\lambda 1560\text{\AA}$ and $\lambda 1657\text{\AA}$) and the stellar continuum is detected down to the shortest wavelength (Fig. 1). The low resolution (~ 2.5 Å) does not allow the stellar emission lines to be resolved. The spectral information is consequently limited to the total line intensity variations. However, this allows for high sensitivity and large spectral coverage to search for many different species in the planetary upper atmosphere.

3. ANALYSIS

To visualize the spectral signature of the transit, we over-plotted off-transit and in-transit spectra (Fig. 2). A significant difference is seen in H I, O I and C II, corresponding to an absorption during the transit. Other spectral lines with about the same intensity do not show the same behaviour (e.g., Si III in Fig. 2). This is the first indication that, in addition to H I, oxygen and carbon are also present in the upper atmosphere of HD 209458b.

¹ Institut d’Astrophysique de Paris, CNRS, 98bis boulevard Arago, F-75014 Paris, France; alfred@iap.fr, desert@iap.fr, lecaveli@iap.fr, hebrard@iap.fr, ehrenrei@iap.fr, ferlet@iap.fr

² Lunar and Planetary Laboratory, Univ. of Arizona, 1040 E. 4th St., Rm 901, Tucson, Arizona 85721-0077, USA; gilda@vega.lpl.arizona.edu

³ Department of Earth and Atmospheric Science, York University, North York, Ontario, Canada; jack@nimbus.yorku.ca

⁴ Observatoire de Genève, CH-1290 Sauverny, Switzerland; michel.mayor@obs.unige.ch

⁵ Jet Propulsion Laboratory/California Institute of Technology and the NASA Astrobiology Institute, MS 150-21, 1200 E. California Blvd. Pasadena, CA 91125, USA; cdp@gps.caltech.edu

To quantitatively estimate the absorptions, their level of detection and error bars, we fitted transit profiles to the measured intensity of each line in each exposure as a function of the orbital phase. The depth and width of the transit curve are related to R_{abs}/R_* , the ratio of the occulting object and stellar radii. The absorption depth due to the planetary disk is $(R_{\text{abs}}/R_*)^2 \sim 1.5\%$. The duration of the ingress and egress of the occultation (i.e. the width of the transit curve) is taken to be proportional to R_{abs} . The term R_{abs}/R_* is the first free parameter of the fit.

The intensity of the emission lines shows detectable variations from one HST visit to another. These variations are interpreted as stellar variations, known to occur in a solar type star at a few percent level on a time scale of several days. To extract the transit signature from these intrinsic variations, we consider the lines intensity as a free parameter for each of the 4 visits. We have thus 4 additional free parameters for each spectral line. The intrinsic stellar variations are found to be at a level of only a few percent between different visits.

The stellar emissions during 3 consecutive exposures of a given HST visit are assumed to be constant. We consider unlikely that short time-scale variations could mimic a transit curve in H_I, O_I and C_{II} and not in the other lines, particularly those of the more ionized species for which more pronounced stellar variations should be observed.

We measured the total line intensities after subtraction of the stellar continuum. The resulting 12 measurements have been fitted as a function of the orbital phase by an occultation curve with five free parameters. Results are shown in Fig. 3 and summarized in Table 1. The full continuum spectrum from 1350Å to 1700Å shows a transit detection with a depth of $2.0^{+0.5}_{-0.7}\%$. In lines, only H_I, O_I and C_{II} show a detection at more than 2σ with transit depths of $5\pm2\%$ in H_I, $13\pm4.5\%$ in O_I and $7.5\pm3.5\%$ in C_{II} (2.6 , 2.6 and 2.1σ detection, respectively). The total squared difference between the line intensities and the fits are found to have values of 8.9 , 9.6 and 4.7 (for H_I, O_I and C_{II}, respectively), in agreement with a χ^2 distribution with 7 degrees of freedom. The other stellar features do not show detectable signatures during transit.

A 10% depth corresponds to a radius R_{abs} of about 3.6 Jupiter radii, which is also the radius of the Roche lobe. The measured absorption depths in O_I and C_{II} correspond to absorbing clouds with a size of several planetary radii. The present detections show that oxygen and carbon are present in the extended upper atmosphere; O_I is even present up to about the level of the Roche lobe.

4. DISCUSSION: OBSERVATIONAL RESULTS

4.1. Continuum

The detection of an absorption of $2.0^{+0.5}_{-0.7}\%$ over the continuum validates the adopted procedure. This absorption is due to the transit of the planetary disk and is known to be $\sim 1.5\%$, well within our error bar. This shows that the systematic errors are significantly below this level.

4.2. Atomic hydrogen

Vidal-Madjar et al. (2003) detected an H_I absorption depth of $15\pm4\%$ over the Lyman- α line. The absorption is significantly detected over only part of the Lyman- α line within a radial velocity range from -130

to 100 km s^{-1} (Fig. 2 of Vidal-Madjar et al. 2003). The $15\pm4\%$ absorption in that spectral range corresponds to about $5.7\pm1.5\%$ absorption of the total Lyman- α line intensity. The H_I absorption depth measured here is consistent with the results of Vidal-Madjar et al. (2003).

4.3. Oxygen and carbon

The O_I stellar emission triplet is a blend of the ground level line at 1302.2Å with the lines from excited levels O_I* and O_I** ($\lambda=1304.9\text{ \AA}$, energy level $E=158\text{ cm}^{-1}$ and $\lambda=1306.0\text{ \AA}$, $E=227\text{ cm}^{-1}$, respectively). The O_I ground level line is strongly absorbed by the interstellar medium (Fig. 2). Therefore the $\sim 13\%$ absorption observed during the transit in the full O_I triplet must be due to the presence of O_I* and O_I** within several planetary radii around the planet, up to about the radius of the Roche lobe. Because these excited levels of O_I are likely populated by collisions, the H_I density at this altitude should be at least the density of a typical exobase, that is about 10^6 cm^{-3} . Assuming solar abundances, such a density is needed for the O_I triplet to have enough opacity to be detected in a line of sight grazing the planet. In these conditions, only the strongest lines of the most abundant species in the most abundant ionization state can be detected, i.e. H_I, O_I and C_{II} (C_I is ionized above 11.3 eV).

Seen at low resolution, the stellar C_{II} line is also a blend of a ground level line from C_{II} ($\lambda=1334.5\text{ \AA}$) with a line from C_{II}* ($\lambda=1335.7\text{ \AA}$, $E=63.42\text{ cm}^{-1}$). Since the ground level C_{II} line is only partially absorbed by the interstellar medium (Fig. 2), at the present low spectral resolution, we cannot a priori discriminate between absorption by C_{II} or C_{II}*. However, for densities above $\sim 20\text{ cm}^{-3}$ (Wood & Linsky 1997), C_{II}* is expected to be collisionally populated, we thus conclude that the detected absorption is due to the presence of both C_{II} and C_{II}* in the extended upper atmosphere of HD 209458b.

Due to the lack of spectral resolution, the real absorption depth over a wavelength limited domain of an emission line (which is linked to the size of the occulting cloud) can be different from the measured absorption depth over the full stellar emission intensity (Sect. 4.2). The measured decrease in intensity depends on the velocity dispersion of the absorbing species compared to the intrinsic width of the stellar emission lines. HD 209458 being a solar type star, we can use the Sun as observed by the SUMER instrument as a reference; the width of the O_I and C_{II} stellar lines must be about $\sim 15\text{ km s}^{-1}$ for O_I and $\sim 25\text{ km s}^{-1}$ for C_{II} (Chae et al. 1998; P. Lemaire, private communication). These values are consistent with the high resolution echelle spectra of HD 209458 (Fig. 2). Therefore, in the absorbing cloud, velocity dispersions of, for example, 25 , 15 and 3 km s^{-1} lead to corrected absorption depths of $13\pm4.5\%$, $13\pm4.5\%$ and $65\pm23\%$ for O_I and $7.5\pm3.5\%$, $12.5\pm6\%$ and $62.5\pm30\%$ for C_{II}, respectively. Note that we obtain similar absorption depths for O_I and C_{II} for velocity dispersions below $\sim 15\text{ km s}^{-1}$.

5. THE ESCAPE MECHANISM

As shown by Vidal-Madjar et al (2003), hydrogen atoms are escaping away from HD 209458b. This has been further discussed by Hébrard et al. (2003), Lammer et al.

(2003), Liang et al. (2003; 2004), Lecavelier des Etangs et al. (2004) and Yelle (2004). The present detection of oxygen and carbon at high altitudes provides additional information about the type of escape mechanism involved. First, oxygen is present up to about the Roche lobe where the H I density must be at least 10^6 cm^{-3} . Second, the absorption depths of oxygen and carbon are related to their velocity dispersion, with $\sim 13\%$ depth for 15 km s^{-1} velocity dispersion and $\sim 65\%$ depth for 3 km s^{-1} .

5.1. Jeans escape

In the frame of Jeans escape, atoms and molecules diffuse upward from the base of the thermosphere up to the exobase level above which the absence of collision allows particles with large velocities in the tail of the Maxwellian distribution to escape. In the thermosphere, the scale height of H I is of the order of 10 000 km (0.1 planetary radius). Under molecular diffusion conditions, the O I scale height is 16 times smaller than the H I one. For an altitude increase of one H I scale height, the O/H ratio decreases by a factor e^{16}/e . Therefore, if molecular diffusion dominates no O I can be detected at high altitudes.

However, in the solar system planetary atmospheres, eddy diffusion is able to transport upward species within the thermosphere up to some level where molecular diffusion takes over. This transport mixes the species, and their abundances remain unchanged upward. Assuming an extreme case of eddy transport up to the Roche lobe or to the exobase, oxygen and carbon abundances should be solar at that level. However even with eddy diffusion and upper atmospheric temperature $T_{\text{up}} \sim 10 000 \text{ K}$ (Lecavelier des Etangs et al. 2004), thermal broadening of absorption lines are $\sim 13 \text{ km s}^{-1}$ for H I, and only $\sim 3 \text{ km s}^{-1}$ for O I and C II. This is smaller by a factor of $\gtrsim 5$ than the width of the stellar lines. If the absorption width was limited by the thermal broadening, the observed $\sim 10\%$ absorption would correspond to a geometrical absorption of more 60%. This would imply that oxygen and carbon extend much further than H I, which is unlikely. Eddy diffusion transport cannot explain the properties of the absorption in O I and C II.

5.2. Hydrodynamic escape: “blow-off”

To explain the present observation, we need a mechanism able to transport oxygen and carbon up to about

the Roche lobe and to maintain their velocity dispersion to at least $\sim 10 \text{ km s}^{-1}$. When an abundant species like H I escapes with a high rate, other species can be dragged up by the hydrodynamical flow, also called “blow-off” (see, e.g., Chamberlain & Hunten 1987). Under such conditions, oxygen and carbon moving out with the H I flow should present a velocity dispersion at least similar to or greater than the sound speed, which is $\sim 10 \text{ km s}^{-1}$ at 10 000 K, i.e. transsonic (Parkinson et al. 2004). The abundances of oxygen and carbon should also be preserved upward all along the flow. Under these conditions, the amounts of O I and C II are large enough to absorb the whole stellar line, allowing at least 10% absorption if they flow up to the Roche lobe. Although the O I and C II absorptions are compatible within the error bars, the dynamical “blow-off” could also explain the apparent lower absorption in carbon as the C II stellar emission line is broader than the H I sound speed by a factor of ~ 2 . In short, the depth of the O I and C II absorptions can be interpreted through the absorption by oxygen and carbon flowing away in a hydrodynamic escape of the atmospheric hydrogen.

6. CONCLUSION

The still unique case of the planet HD 209458b transiting a bright star has allowed the first studies of an extra-solar planet atmosphere. The detection of oxygen (at 2.6σ) and carbon (at 2.1σ), a signature of an atmospheric “blow-off”, shows that, as already suggested by Hébrard et al. (2003) and Vidal-Madjar & Lecavelier des Etangs (2003) hot-Jupiters can lose a significant fraction of their atmosphere. Ultimately, such a process could lead to a new type of planets with hydrogen-poor atmosphere, or even with no atmosphere at all (see Trilling et al. 1998).

We thank the Egyptian god Osiris for suggesting his name for the planet (Vidal-Madjar & Lecavelier des Etangs 2003). Based on observations obtained with the NASA/ESA Hubble Space Telescope operated by the Association of Universities for Research in Astronomy, Inc., under NASA contract NAS 5-26555. We thank S. Beckwith for allocating us Director Discretionary time. C. D. P. acknowledges support by the NASA through the Astrobiology Institute under Cooperative Agreement No. CAN-00-OSS-01 and issued through the Office of Space Science.

REFERENCES

Chae, J., Schuhle, U., & Lemaire, P. 1998, ApJ, 505, 957
 Chamberlain, J. W., & Hunten, D. M. 1987, in *Theory of planetary atmospheres*, Internat. Geophys. Ser., 36
 Charbonneau, D., Brown, T. M., Latham, D. W., & Mayor, M. 2000, ApJ, 529, L45
 Charbonneau, D., Brown, T. M., Noyes, R. W., & Gilliland, R. L. 2002, ApJ, 568, 377
 Désert, J.-M., et al. 2003, in *Extrasolar planets: today and tomorrow*, ASP Conf. Ser., in press (astro-ph/0312383)
 Hébrard, G., et al. 2003, in *Extrasolar planets: today and tomorrow*, ASP Conf. Ser., in press (astro-ph/0312384)
 Henry, G. W., Marcy, G. W., Butler, R. P., & Vogt, S. S. 2000, ApJ, 529, L41
 Lammer, H., Selsis, F., Ribas, I., Guinan, E. F., Bauer, S. J., & Weiss, W. W. 2003, ApJ, 598, L121
 Lecavelier des Etangs, A., Vidal-Madjar A., McConnell, J. C., & Hébrard, G. 2004, A&A submitted
 Liang, M., Parkinson, C. D., Lee, A. Y.-T., & Yung, Y. L., & Seager, S. 2003, ApJ, 596, L247
 Liang, M., Seager, S., Parkinson, C. D., Lee, A. Y.-T., Yung, Y. L. 2004, ApJL, submitted
 Mazeh, T., Naef, D., Torres, G., et al. 2000, ApJ, 532, L55
 Parkinson, C. D., Richardson, M. I., & Kasting, J. 2004, in prep.
 Trilling, D. E., Benz, W., Guillot, T., et al. 1998, ApJ, 500, 428
 Vidal-Madjar, A., & Lecavelier des Etangs, A. 2003, in *Extrasolar planets: today and tomorrow*, ASP Conf. Ser., in press (astro-ph/0312382)
 Vidal-Madjar, A., Lecavelier des Etangs, A., Désert, J.-M., et al. 2003, Nature, 422, 143
 Watson, A. J., Donahue, T. M., & Walker, J. C. G. 1981, Icarus, 48, 150
 Wood, B. E., & Linsky, J. L. 1997, ApJ, 474, L39
 Yelle, R. V. 2004, Icarus, submitted

TABLE 1
ABSORPTION DEPTH OF EMISSION LINES AND CONTINUUM

Species	λ^a (Å)	Absorption depth ^b	
		1σ (%)	2σ (%)
Continuum	1350-1700	$2.0^{+0.5}_{-0.7}$	
H I	1212-1220	$5.3^{+1.6}_{-1.9}$	
O I, O I*, O I**	1300-1310	$12.8^{+4.5}_{-4.5}$	
C II, C II*	1332-1340	$7.5^{+3.6}_{-3.4}$	
C I	1557-1565	$0.4^{+21.1}_{-0.4}$	<36.0
C I	1654-1660	$11.3^{+11.9}_{-11.3}$	<33.6
C IV	1545-1554	$0.4^{+9.5}_{-0.4}$	<19.0
N V	1237-1246	$27.3^{+22.7}_{-27.3}$	<50.0
S I, S I*, S I**	1471-1489	$32.2^{+13.0}_{-32.2}$	<58.2
S II, S II*	1525-1536	$18.4^{+15.4}_{-18.4}$	<47.4
S III	1204-1210	$0.0^{+2.2}_{-0.0}$	<5.9
S IV	1391-1397	$0.0^{+6.5}_{-0.0}$	<14.0

^a Wavelength range for the lines intensity evaluation.

^b Absorption depth given by the $(R_{\text{abs}}/R_*)^2$ parameter of the fit (see text).

1- σ error bars and 2- σ upper limits for non-detections.

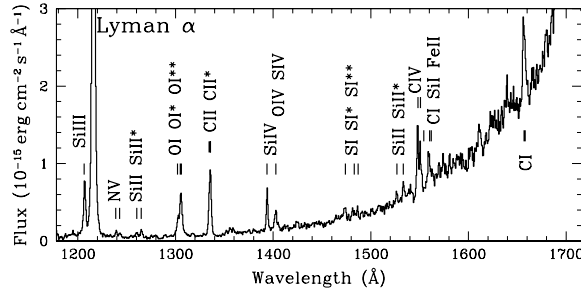


FIG. 1.— The full HD 209458 G140L spectrum. Stellar emission lines are clearly detected together with the stellar continuum which is increasing towards longer wavelengths.

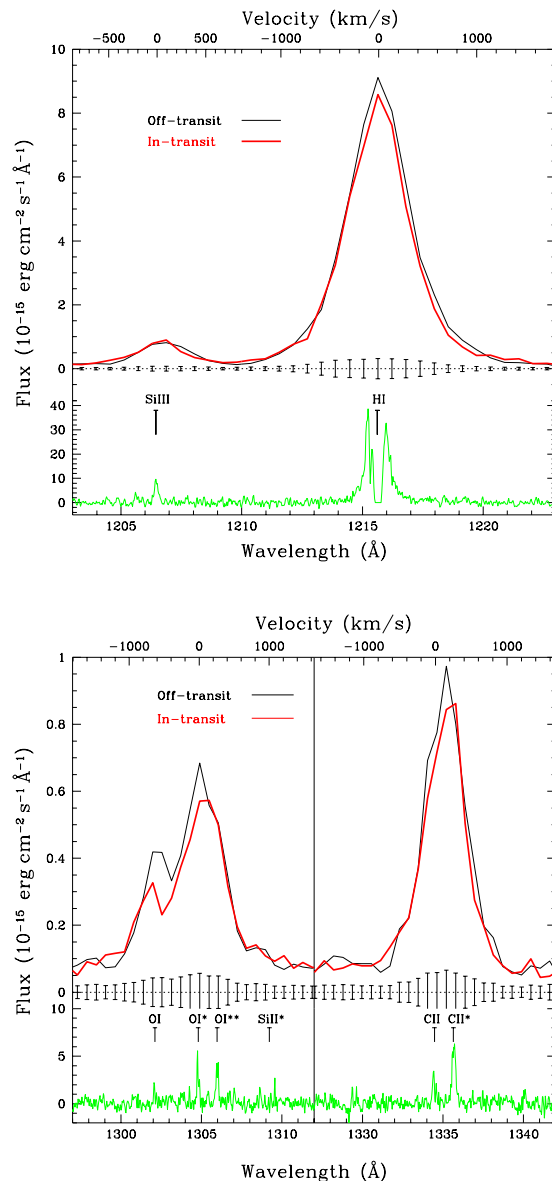


FIG. 2.— Comparison of off-transit and in-transit spectra for the SiIII, H1, O1 and CII lines with $1-\sigma$ error bars. The off-transit spectrum is the addition of the first exposure of the 1st and 3rd visits (thin lines); the in-transit corresponds to the addition of the fully in-transit exposure of each of the four HST visits (thick lines). Absorption is clearly detected in the H1, O1 and CII lines. No signal is detected in other lines (e.g., SiIII) with about the same amplitude. The bottom panels show the high resolution spectra obtained in 2001 with the echelle grating (Vidal-Madjar et al. 2003).

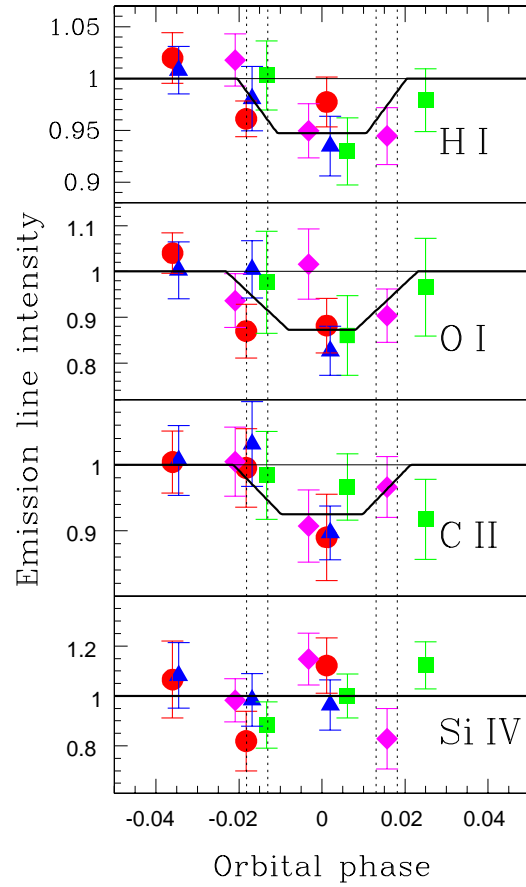


FIG. 3.— Plot of the lines total intensity as a function of the orbital phase. Circles, squares, triangles and diamonds are for 1st to 4th transits respectively. The vertical dotted lines corresponds to the position of the 1st to 4th contacts of the planetary disk transit. The thick line represents the best fit to the data (see Sect. 3). Absorptions are detected in H I, O I and C II during the transits; no significant absorptions are detected in the other lines (i.e. Si IV).